JOURNAL OF PROPULSION AND POWER
Vol. 24, No. 2, March–April 2008

Multiple Surrogate Modeling for Axial Compressor Blade Shape Optimization

Abdus Samad* and Kwang-Yong Kim†
Inha University, Incheon 402-751, Republic of Korea
Tushar Goel‡ and Raphael T. Haftka§
University of Florida, Gainesville, Florida 32611
and
Wei Shyy¶
University of Michigan, Dearborn, Michigan 48128

DOI: 10.2514/1.28999

A major issue in surrogate model-based design optimization is the modeling fidelity. An effective approach is to employ multiple surrogates based on the same training data to offer approximations from alternative modeling viewpoints. This approach is employed in a compressor blade shape optimization using the NASA rotor 37 as the case study. The surrogate models considered include polynomial response surface approximation, Kriging, and radial basis neural network. In addition, a weighted average model based on global error measures is constructed. Sequential quadratic programming is used to search the optimal point based on these alternative surrogates. Three design variables characterizing the blade regarding sweep, lean, and skew are selected along with the three-level full factorial approach for design of experiment. The optimization is guided by three objectives aimed at maximizing the adiabatic efficiency, as well as the total pressure and total temperature ratios. The optimized compressor blades yield lower losses by moving the separation line toward the downstream direction. The optima for total pressure and total temperature ratios are similar, but the optimum for adiabatic efficiency is located far from them. It is found that the most accurate surrogate did not always lead to the best design. This demonstrated that using multiple surrogates can improve the robustness of the optimization at a minimal computational cost.

I. Introduction

IN RECENT years, shape optimization based on three-dimensional flow analysis has been performed in turbomachinery blade shape design, as demonstrated by Papila et al. [1], Gallimore et al. [2], Ahn and Kim [3], Jang and Kim [4], Jang et al. [5,6], Yi et al. [7], Benini and Biollo [8], and Oyama et al. [9], for example. They have investigated compressor optimization for aircraft engine applications using lean and skewed blades for efficiency enhancement.

Surrogate-based approximations are being increasingly used in single or multidisciplinary optimizations. Considering the competing requirements of computational economy, that is, employing as few data points as possible for constructing a surrogate mode, and fidelity, that is, offering high accuracy in representing the characteristics of the design space, the assessment of the performance of surrogate models is of critical importance. Queipo et al. [10] and Li and Padula [11] reviewed various surrogate-based models used in mostly aerospace applications. Shyy et al. [12] applied response surface approximation (RSA) and radial basis neural network (RBNN) techniques to rocket engine design by comparing the prediction of alternative models. Zerpa et al. [13] presented a multiple surrogate model, that is, a weighted average surrogate model based on RSA, RBNN, and Kriging models. They determined weights for the weighted average model considering only pointwise estimation of the variance for the three surrogate models. Goel et al. [14] also developed a global version of the weighted average surrogate models using RSA, RBNN, and Kriging models, in which the weights are fixed and determined according to cross-validation errors. The larger the error in prediction produced by any surrogate, the smaller the weight is assigned to that surrogate to construct the weighted average model. They concluded that the weighted average surrogate model is a more reliable prediction method than individual surrogates. Because the same training data can be repeatedly used, the cost of constructing multiple surrogates from the same simulation data is very small; it seems desirable to produce multiple optima to increase the likelihood of reaching the best outcome. Goel et al. [15] demonstrated the application of this approach to optimal model calibration in cryogenic cavitation.

The present work aims to demonstrate the advantage of using multiple surrogates as well as the weighted surrogate model of Goel et al. [14] in the shape optimization of a transonic axial compressor blade. Geometric variables related to the sweep, lean, and skew of the blade are selected as design variables, and adiabatic efficiency, total pressure, and total temperature are selected as objective functions. The basic surrogate models, that is, RSA, RBNN, and Kriging models, as well as the multiple surrogate model, have been evaluated for their efficiency in predictions.

II. Problem Description and Numerical Procedure

A. Blade Geometry and Flow Parameters

NASA rotor 37 (Reid and Moore [16]), an axial-flow compressor rotor with a low-aspect ratio, is used for blade shape optimization in the present study. The detailed specifications of the compressor are summarized in Table 1. The rotor tip clearance is 0.356 mm (0.45% span). The measured choking mass flow rate is 20.93 kg/s, which corresponds to 103.67% of the design flow rate (20.19 kg/s).

Received 24 November 2006; revision received 21 August 2007; accepted for publication 31 August 2007.

*Graduate Student, Department of Mechanical Engineering, 253 Yonghyun-Dong, Nam-Gu.
†Professor, Department of Mechanical Engineering, 253 Yonghyun-Dong, Nam-Gu; kykim@inha.ac.kr. Member AIAA.
‡Graduate Student, Department of Mechanical and Aerospace Engineering. Student Member AIAA.
§Professor, Department of Mechanical and Aerospace Engineering. Fellow AIAA.
¶Professor and Chair, Department of Aerospace Engineering. Fellow AIAA.

Table 1 Design specifications of NASA rotor 37

Mass flow, kg/s	20.19
Rotational speed, rpm	17190
Pressure ratio	2.106
Inlet hub-tip ratio	0.7
Inlet tip relative Mach no.	1.4
Inlet hub relative Mach no.	1.13
Tip solidity	1.29
Rotor aspect ratio	1.19
No. of rotor blades	36

The meridional view of the axial compressor is shown in Fig. 1. Total pressure and total temperature with relation to the mass flow rates are measured at inlet (station 1) and outlet (station 2) positions. The inlet and outlet positions are located at 41.9 mm upstream of the tip leading edge of the rotor and at 101.9 mm downstream of the tip trailing edge of the rotor, respectively.

The three-dimensional thin-layer Navier–Stokes and energy equations are solved on a body-fitted grid using the explicit Runge–Kutta scheme proposed by Jameson et al. [17] from initial to steady state with a spatially varying time step to accelerate convergence. Artificial dissipation terms have been added to resolve shocks. The algebraic turbulence model of Baldwin and Lomax [18] has been employed to estimate the eddy viscosity.

Figure 2 shows computational grids. A composite grid system with structured H-, C-, and O-type grids is adopted to represent the complicated configuration of the axial compressor. The H-type grid consists of $60 \times 36 \times 63$ points (in the streamwise, pitchwise, and spanwise directions, respectively) and is introduced for the inlet flow region. A C-type grid consisting of $350 \times 46 \times 63$ points is used for the blade passage. The grid embedded in the tip clearance consists of $182 \times 13 \times 13$ points. The whole grid system has about 1,181,000 grid points. The average number of iterations and CPU time for the converged solution are approximately 3000 and 3.5 h, respectively, using a NEC SX-6 (144 GFLOPS) supercomputer.

The Mach numbers in each direction, total pressure, and total temperature are given at the inlet. At the exit, the hub static pressure ratio has been specified, and the radial equilibrium equation is solved along the blade span. A periodic tip clearance model is used to resolve the tip clearance flow explicitly. The no-slip and adiabatic wall conditions are used at all the wall boundaries. For reducing the computational load, flowfield in a single blade passage is simulated by applying periodic boundary conditions in the tangential direction.

B. Validation of Numerical Simulation

For the validation of the present numerical solutions, Fig. 3 shows the comparison between computational and experimental distributions of adiabatic efficiency with respect to mass flow rate. The symbols, squares and circles, indicate the results of Reynolds-averaged Navier–Stokes (RANS) calculations for reference and optimal shapes, respectively. In the figure, the mass flow rates are normalized with the choking flow rate (20.93 kg/s) obtained from the experiment (Reid and Moore [16]). It is noted that the horizontal axis has a narrow range around the design flow condition (mass flow rate/choked mass flow rate = 0.965) because flow characteristics in the present study are only considered at the design flow condition. At the design flow rate (design mass flow/choked mass flow rate = 0.965 in Fig. 3), the adiabatic efficiency obtained by the numerical analysis for the reference blade is only 1.3% higher than the experimental efficiency. Further validations of the present numerical procedure are available in [3–6].

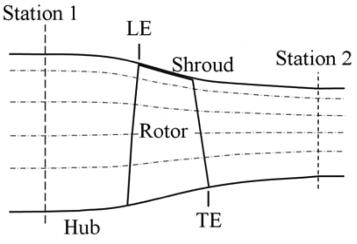

Fig. 1 Meridional view of rotor 37.

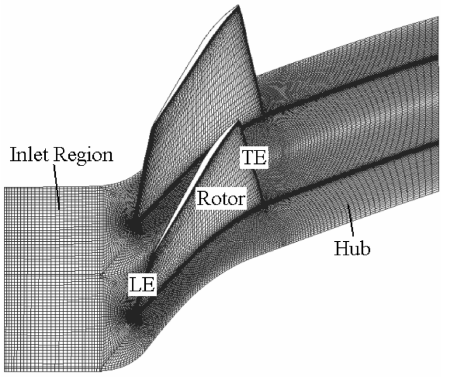

a) Perspective view

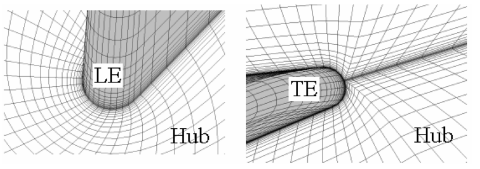

b) View from casing at LE and TE of hub

Fig. 2 Computational grids.

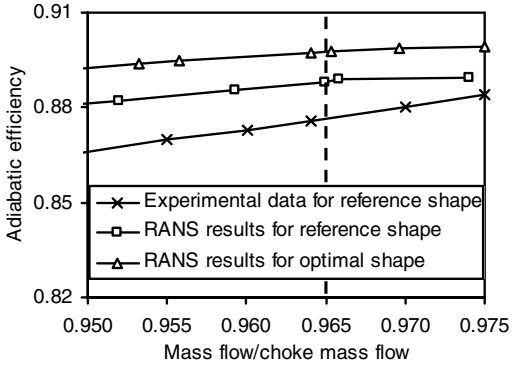

Fig. 3 Adiabatic efficiency according to normalized mass flow rates (vertical dotted line: design flow rate).

C. Objective Functions and Design Variables

In the present study, the adiabatic efficiency, total temperature ratio, and total pressure ratio are selected as objective functions of the shape optimization of the rotor blades. To improve the overall efficiency, the objective function is defined as

$$F_1 = 1 - \eta_{\text{ad}}, \qquad \eta_{\text{ad}} = \frac{(P_{0\text{exit}}/P_{0\text{inlet}})^{(k-1)/k} - 1}{T_{0\text{exit}}/T_{0\text{inlet}} - 1} \tag{1}$$

where η_{ad} is adiabatic efficiency, k is the ratio of specific heats, and P_0 and T_0 are the total pressure and total temperature, respectively. The subscripts, inlet and exit, indicate sections 1 and 2 in Fig. 1, respectively. The total temperature ratio (F_2) and total pressure ratio (F_3) are also tested as objective functions for shape optimization, as follows:

$$F_2 = T_{0\text{exit}}/T_{0\text{inlet}} \tag{2}$$

$$F_3 = P_{0\text{exit}}/P_{0\text{inlet}} \tag{3}$$

where the location of the inlet is not the same as in Eq. (1) and corresponds to the location of the inlet of the C grid in Fig. 2. The

intention of optimization is to increase the efficiency (therefore, to reduce efficiency-based objective function, F_1), total temperature ratio, and total pressure ratio.

High temperature rise in a stage is desirable to minimize the number of stages for a given overall pressure ratio in a compressor, provided that one can maintain the same efficiency. Hence, as proposed in the present study, it is important to address the total temperature and pressure rise along with the efficiency consideration. To attain a higher total temperature rise, the designers must combine high blade speed, high axial velocity and high fluid deflection in the rotor blade. High blade speed is limited due to blade stress as well as aerodynamic reasons, and high axial velocity and high fluid deflection are limited due to adverse pressure gradient. The same set of experimental designs are used to obtain the response data for the three objectives. Thus, inevitably, some optimum points are located at the boundary of the design space.

Multi-objective optimization to compromise between efficiency and total pressure is also considered by employing the following objective function:

$$F = \eta_{ad} + w_f P_{0exit}/P_{0inlet} \tag{4}$$

where w_f is a weighting factor specified by the designer.

Three design variables are selected in these optimizations: one for sweep, another for lean, and the other for skew. In Figs. 4–6, the definitions of the variables are presented. Blade sweep, α in Fig. 4, is defined at the rotor tip and normalized by the axial tip chord (=27.77 mm). The airfoil sections are moved toward the downstream direction for positive sweep (α). The line of the swept blade between the rotor tip and hub is linearly connected and the tip clearance gap is kept constant.

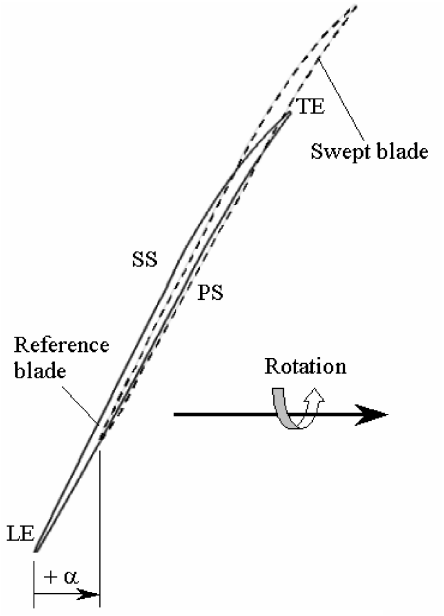

a) Top view

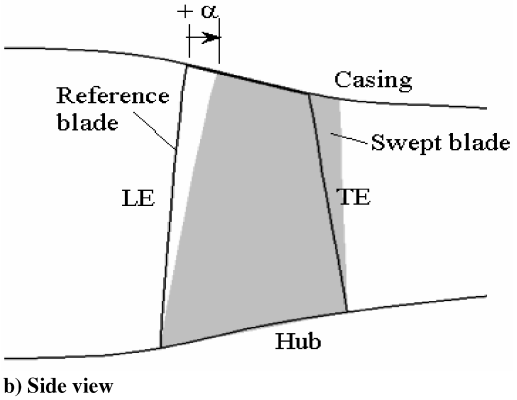

b) Side view

Fig. 4 Definition of blade sweep.

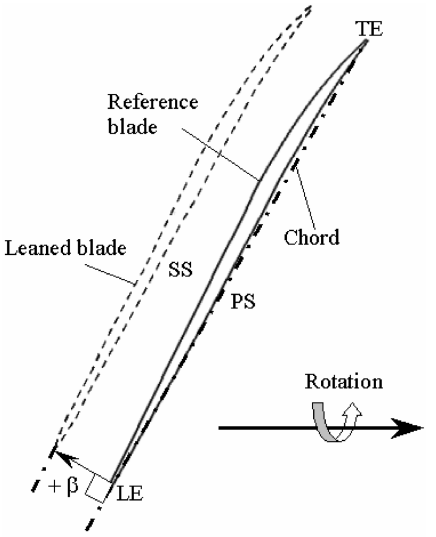

Fig. 5 Definition of blade lean (top view).

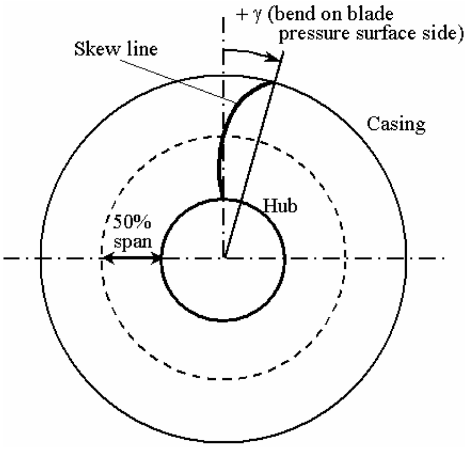

Fig. 6 Definition of blade skew (front view).

The blade lean is shown in Fig. 5 from the top view. Lean is defined as the movement of the aerofoil normal to the chord line at the tip. Lean also is normalized by the axial tip chord. Here, lean (β) is taken as positive if the aerofoil sections are moved toward the blade suction surface side. Lean (β) is taken as zero at the hub, and the blade lean is linearly connected from hub to tip and the tip clearance is kept constant.

Figure 6 presents the skewed blade stacking line, and a single skew angle (γ) is defined only at the rotor tip. If the blade bends toward the pressure surface side, the skew angle is taken as positive. The skew line is defined as a second-order polynomial. The constants and the coefficients are found by the constraints; the skew angle is zero at both hub and midspan, and γ at tip of the blade.

Ranges of the variables are selected based on preliminary calculations and prior experiences. The boundary and the midpoints of the range are prescribed for each design variable, as in Table 2.

Table 2 Design ranges of blade sweep, lean, and skew

Variables	Lower bound	Middle	Upper bound
Sweep	0.0	0.13	0.25
Lean	−0.036	−0.018	0.000
Skew (radian)	0.0	0.05	0.1

III. Optimization Methodology

The optimization procedure is described in a flowchart shown in Fig. 7. Initially, the variables are selected and the design space is decided for improvement of system performance. Using the design of experiment (DOE) technique (Myers and Montgomery [19]), the design points are selected, and at these design points the objective functions are calculated using the flow solver. In this work, the DOE is conducted using a three-level full factorial design. A full factorial design with 27 points was used. Three of the analyses did not converge and the other 24 were used to fit the surrogate. Evaluations of the objective functions at these design points are carried out by three-dimensional RANS analysis.

The next steps are to construct the surrogates and to find the optimal points. The optimal points are found separately for all the surrogates using sequential quadratic programming. Furthermore, for F_1, if the optimal points are found to touch any boundary of the design space, it is checked and the range is adjusted. Although the same practices can be done for other objectives, it is not necessary in the present study. The surrogate methods used in this work are described next.

A. Response Surface Approximation Model

In the response surface approximation method (Myers and Montgomery [19]), the following polynomial function is fitted to get the response surface approximation. If the regression coefficients are βs, the polynomial function becomes

$$\hat{F} = \beta_0 + \sum_{j=1}^{n} \beta_j x_j + \sum_{j=1}^{n} \beta_{jj} x_j^2 + \sum \sum_{i \neq j}^{n} \beta_{ij} x_i x_j \tag{5}$$

where n is the number of design variables and x represents the design variables.

B. Radial Basis Neural Network Model

The radial basis neural network (Orr [20]) is a two-layer network that consists of a hidden layer of radial basis function and a linear output layer. The parameters for fitting this surrogate model are spread constant and a user defined error goal. The allowable error goal is decided from the allowable error from the mean input responses. In MATLAB [21], *newrb* is the function for the RBNN network design.

C. Kriging Model

Kriging model (Martin and Simpson [22]) is an interpolating meta-modeling technique that employs a trend model $f(x)$ to capture large-scale variations and a systematic departure $Z(x)$ to capture small-scale variations. Kriging postulation is the combination of the global model and departures of the following form:

$$\hat{F}(x) = f(x) + Z(x) \tag{6}$$

where $\hat{F}(x)$ represents the unknown function and $f(x)$ is the global model, whereas $Z(x)$ represents the localized deviations. $Z(x)$ is the realization of a stochastic process with mean zero and nonzero covariance. A linear polynomial function is used as a trend model and the systematic departure terms follow Gaussian correlation function.

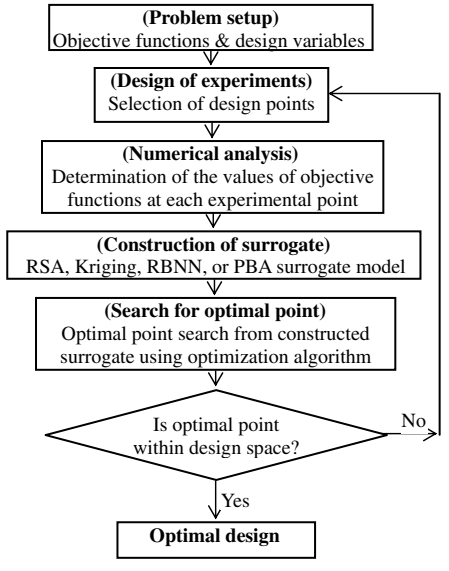

Fig. 7 Optimization procedure.

D. Weighted Average Model

A weighted average model proposed by Goel et al. [14] is adopted in the present investigation. It is based on the PRESS-based-averaging (PBA) model (termed WTA3 by Goel et al. [14]). The predicted response is defined as follows for the PBA model:

$$\hat{F}_{\text{wt.avg}}(x) = \sum_{i}^{N_{\text{SM}}} w_i(x) \hat{F}_i(x) \tag{7}$$

where N_{SM} is the number of basic surrogate models used to construct the weighted average model. The ith surrogate model at design point x produces weight $w_i(x)$, and $\hat{F}_i(x)$ is the predicted response by the ith surrogate model.

Weights are decided such that surrogates that produce high error have low weight and thus low contribution toward the final weighted average surrogate, and vice versa. In this work, global weights are selected using a generalized mean square cross-validation error (GMSE), or PRESS (in RSA terminology), that is a global data-based measure of goodness. A generalized mean square cross-validation error calculation procedure is given in the Appendix.

The weighting scheme used in a PRESS-based averaging surrogate is given as follows:

$$\begin{aligned} w_i^* &= (E_i/E_{\text{avg}} + \alpha)^{\beta}, \qquad w_i = w_i^* \Big/ \sum_i w_i^* \\ E_{\text{avg}} &= \sum_{i=1}^{N_{\text{SM}}} E_i/N_{\text{SM}}; \qquad \beta < 0, \alpha < 1 \\ E_i &= \sqrt{\text{GMSE}_i}, \qquad i = 1, 2, \ldots, N_{\text{SM}} \end{aligned} \tag{8}$$

Two constants α and β are chosen as $\alpha = 0.05$ and $\beta = -1$ (Goel et al. [14]).

Next RSA, Kriging, RBNN, and PBA surrogate models are constructed using objective function values at design points. Equations (7) and (8) are used to construct the weighted average surrogate model. The constructed surrogates are used to search for optimal points using a sequential quadratic programming (function *fmincon* in MATLAB [21]).

IV. Results and Discussion

A. Optimization Results

Tables 3–8 contain the optimization results for the three objective functions with different surrogate models. The optimal variables given in these tables are normalized in the design ranges shown in Table 2, and have the values between 0 and 1. Tables 3, 5, and 7 show the cross-validation errors and calculated weights for each surrogate. The results show that the RSA approach gives the lowest

Table 3 Weights for PBA model to construct weighted average model for F_1

Model	Cross-validation error, E_{cv}	Weight
RBNN	3.09E − 03	0.322
RSA	2.40E − 03	0.409
KRG	3.71E − 03	0.270

Table 4 Optimal designs suggested by various surrogates and corresponding predicted RANS results for objective F_1

Surrogate model		PBA	RBNN	RSA	KRG	Simple average
Optimal design variables	α_{opt} (sweep)	0.442	0.411	0.401	0.465	0.442
	β_{opt} (lean)	0.905	1.000	0.748	0.971	0.916
	γ_{opt} (skew)	0.651	0.615	0.632	0.635	0.652
$F_{surrogate}$		0.0995	0.0994	0.0993	0.0990	0.0995
F_{RANS}		0.1010	0.1008	0.1015	0.1018	0.1011
$F_{RANS} - F_{surrogate}$		1.50E − 03	1.40E − 03	2.20E − 03	2.80E − 03	1.64E − 03
$F_{reference}$				0.1135		
$F_{RANS} - F_{reference}$		−0.0125	−0.0127	−0.0120	−0.0117	−0.0124
Reduction in F_1, %		11.01	11.19	10.57	10.31	−10.93

Table 5 Weights for PBA model to construct weighted average model for objective function, F_2

Model	Cross-validation error, E_{cv}	Weight
RBNN	7.39E − 03	0.359
RSA	6.72E − 03	0.393
KRG	1.09E − 02	0.248

Table 7 Weights for PBA model to construct weighted average model for objective function, F_3

Model	Cross-validation error, E_{cv}	Weight
RBNN	3.73E − 02	0.373
RSA	3.58E − 02	0.388
KRG	5.97E − 02	0.239

cross-validation error among the three individual surrogates, and the Kriging (KRG) technique performs the worst for all three objectives. The low cross-validation error for RSA is likely to indicate that the objectives are modeled well as quadratic polynomials. In PBA, the weight associated with RSA is the largest.

Tables 4, 6, and 8 compare the predictions of the optimal values predicted by different surrogate models against the actual RANS calculation at the corresponding points. Consistent with the aforementioned error estimate, KRG performs the worst. In the case of F_1, RBNN gives the most accurate prediction of optimal objective function value, followed by PBA. But, in both F_2 and F_3, RSA gives the most accurate predictions of the objective functions at the optimal points, and RBNN the next. Depending on the characteristics of the design space in each problem, certain surrogate models can perform more satisfactorily than others. However, it is difficult to tell a priori which surrogate models are more appropriate. These are precisely the merits of adopting multiple surrogates and finding ways to form a more robust composite surrogate, as is done in this study.

It should be pointed out that although the cross-validation error estimate has correctly predicted that KRG is the worst performing surrogate, RSA, with the lowest cross-validation error, does not yield the best performance. The discrepancy between the cross-validation error and actual performance is due to two reasons. First, the cross-validation error is an estimate of the average square error over the entire domain, whereas the optimal designs are found in a small subregion in which one of the surrogates may have an advantage. Second, the cross-validation error is only an estimate of global performance. The multiple surrogate model, PBA, does not show the best performance in any case but it gives satisfactory results in most cases and protects against the worst surrogate (in this case, KRG). Therefore, even though the multiple surrogate models do not necessarily guarantee the best performance, they seem to perform more consistently and, hence, can improve the robustness of optimization results at a minimal computational cost.

The efficiency, total temperature, and total pressure ratios obtained by RANS analyses for the reference shape ($F_{reference}$), that is, NASA rotor 37, are 88.65 % ($F_1 = 0.1135$), 1.2721, and 2.1334, respectively. Table 4 shows that RBNN found the optimum point that gives the largest reduction in F_1, 11.19% (about 1.43% improvement in efficiency), in comparison with the reference shape. And, PBA predicts the optimum point with the second highest efficiency. Whereas in the case of F_2, PBA, RBNN, and RSA show similar performances, that is, 0.22% increase in F_2. RBNN gives the best optimum point with 0.94% increase in F_3, followed by PBA. Therefore, RBNN predicts the best optimum points in all of the cases. It is noted that in the case of F_1, the performances of the surrogate models to predict the optimum point are consistent with the reliabilities of the aforementioned surrogate models in comparison with the RANS predictions. However, in the case of F_3, RSA with the best reliability predicts the worst optimum point.

Except for the weighted average surrogate model, PBA, the surrogate models predict similar optimum points for F_2 and F_3. However, the best efficiency points, that is, the optimum designs for F_1, are very different from the F_2 and F_3 designs as seen by comparing Tables 4, 6, and 8, and also in Fig. 8, which shows the values of objective functions at each optimum point. However, this is quite natural because enhancing the efficiency and reducing the number of compressor stages by increasing the pressure ratio are different tasks. There can be situations with good temperature profiles while terrible in total pressure, an adiabatic shock flow being an example. But, for this compressor application, total temperature and total pressure ratios are expected not much different to each other.

Table 6 Optimal designs suggested by various surrogates and corresponding predicted RANS results for objective F_2

Surrogate model		PBA	RBNN	RSA	KRG	Simple average
Optimal design variables	α_{opt} (sweep)	0.000	0.000	0.000	0.000	0.000
	β_{opt} (lean)	0.676	0.903	0.769	1.000	0.696
	γ_{opt} (skew)	0.044	0.237	0.165	0.392	0.049
$F_{surrogate}$		1.2730	1.2738	1.2744	1.2705	1.2719
F_{RANS}		1.2749	1.2748	1.2748	1.2738	1.2749
$F_{RANS} - F_{surrogate}$		1.90E − 03	1.00E − 03	4.00E − 04	3.30E − 03	2.00E − 03
$F_{reference}$				1.2721		
$F_{RANS} - F_{reference}$		0.0028	0.0027	0.0027	0.0017	0.0028
Increase in F_2, %		0.22	0.22	0.22	0.14	0.22

Table 8 Optimal designs suggested by various surrogates and corresponding predicted RANS results for objective F_3

Surrogate model		PBA	RBNN	RSA	KRG	Simple average
Optimal design variables	α_{opt} (sweep)	0.000	0.000	0.000	0.000	0.000
	β_{opt} (lean)	0.900	0.878	0.768	1.000	0.924
	γ_{opt} (skew)	0.227	0.192	0.195	0.346	0.237
$F_{surrogate}$		2.1473	2.1585	2.1505	2.1345	2.1464
F_{RANS}		2.1525	2.1536	2.1491	2.1494	2.1512
$F_{RANS} - F_{surrogate}$		5.20E − 03	−4.90E − 03	−1.40E − 02	1.49E − 02	4.81E − 03
$F_{reference}$				2.1334		
$F_{RANS} - F_{reference}$		0.0191	0.0202	0.0157	0.016	0.0178
Increase in F_3, %		0.90	0.94	0.74	0.75	0.8343

As for the reliability of the surrogates, further evaluations are made in Fig. 9 and Table 9. Relative errors of surrogate predictions at 12 different optimal points in design space are shown in Fig. 9. As the same set of data is used for the optimization, four surrogate models give 12 total optimal points in design space for the F_1, F_2, and F_3 objectives. And, root-mean-square averaged errors based on RANS calculations and surrogate predictions at these points are given in Table 9. In all of the cases, RSA shows the best accuracy, whereas KRG shows the worst. This is consistent with the results that the cross-validation errors shown in Tables 3, 5, and 7 indicate. In comparison with the aforementioned results at the optimum points (Tables 4, 6, and 8), the surrogates with the best accuracy are the same except for F_1, and the magnitudes of the errors are substantially larger.

To show the sensitivity of weights on PBA, a simple average surrogate model is tested. In this model, all surrogates are weighted equally to construct the model. Tables 4, 6, and 8 show that the results of the simple average model are only slightly inferior to the results of PBA.

The results of optimization with multiple objectives [Eq. (4)] are shown in Fig. 10. The design variables except lean are dependent strongly on the weighting factor, and all of them decrease as the weighting factor increases in the range of the weighting factor shown in Fig. 10a. This means that distortion of the stacking line is effective in the enhancement of the efficiency rather than the total pressure. Figure 10b shows that the total pressure ratio increases as weighting factor increases, just as intended.

Figure 11 shows the limiting streamlines on the blade suction surface for the reference and efficiency optimized blades. In this figure, three solid lines are drawn to present the 10, 75, and 90% spans of the blade. The separation and reattachment lines are generated near the midchord. This separation line appears due to the interference between the passage shock and the suction surface boundary layer. Here, it can be seen that the separation line is moved downstream in the optimized blade. The outward radial flow caused by the centrifugal effect also moves downstream of the separation line.

Figure 12, shown in the perspective view from the casing for the Mach number contours at 10, 75, and 90% spans, depicts the movement of interference position of the passage shock with the blade suction surface boundary layer toward downstream for the optimized blade as compared to that of the reference one. At 10% span, the figure shows that the interference position of the passage shock did not change between the optimized and the reference blades. This can also be seen in Fig. 11, that at 10% span there is not

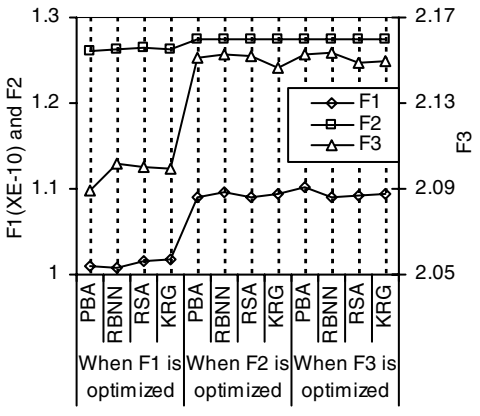

Fig. 8 RANS calculations at the optimum points predicted by different surrogates.

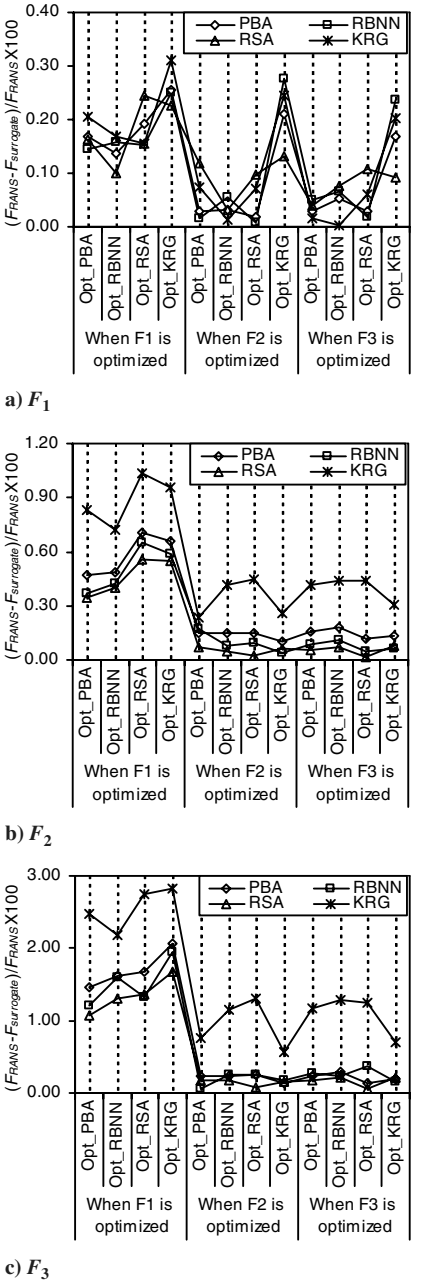

Fig. 9 Errors in predictions of surrogates at different points in the design space.

Table 9 Root-mean-square averaged errors in predictions of the surrogates at 12 optimal points

Surrogates	RMS errors produced by the surrogates		
	F_1	F_2	F_3
PBA	1.24E − 03	4.57E − 03	2.12E − 02
RBNN	1.36E − 03	3.93E − 03	1.93E − 02
RSA	1.20E − 03	3.50E − 03	1.69E − 02
KRG	1.43E − 03	7.60E − 03	3.63E − 02

much difference between the reference and optimized blades for separation and reattachment lines.

The distributions of static pressure on surfaces of optimum blades are shown in Fig. 13. Pressure changes abruptly across the separation line on the suction surface. And, in the case of the efficiency optimized blade, it is noted that near tip of leading edge on pressure surface the pressure shows the minimum whereas the relatively high pressure region is located in this place in the other objective optimized cases. And, also on the suction surface, the efficiency optimized blade shows that the pressure decreases more rapidly as the tip is approached than the other optimum blades. Therefore, it is found from this figure that enhancement of efficiency is achieved by modifying the flow near the tip of the blade. This is consistent with

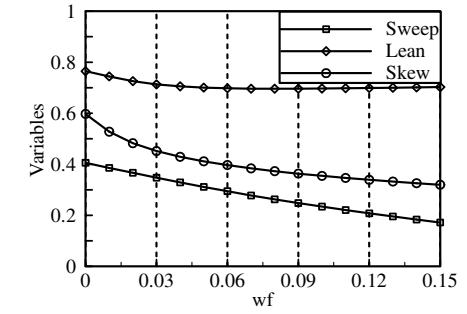

a)

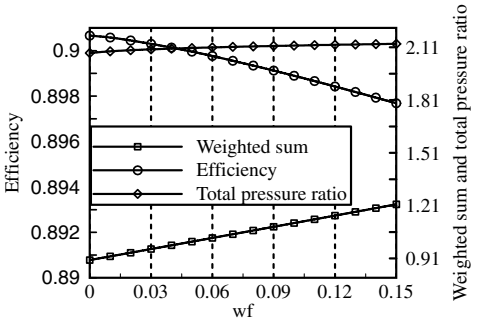

b)

Fig. 10 Results of multiple-objectives optimization: a) design variables, b) objective function values.

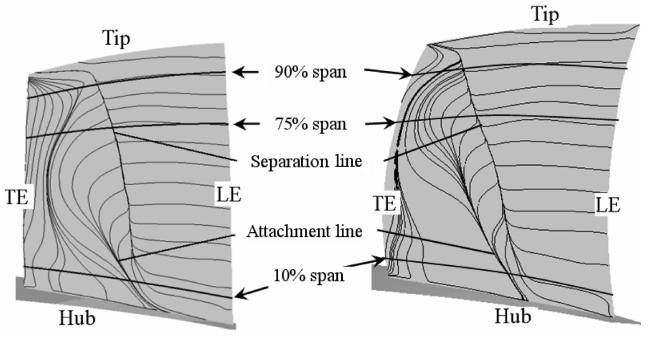

a) Reference blade **b) Efficiency optimized blade**

Fig. 11 Limiting streamlines on the blade suction surface.

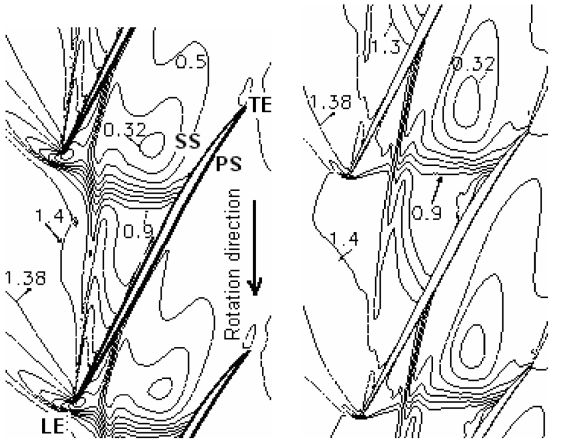

a) 90% span

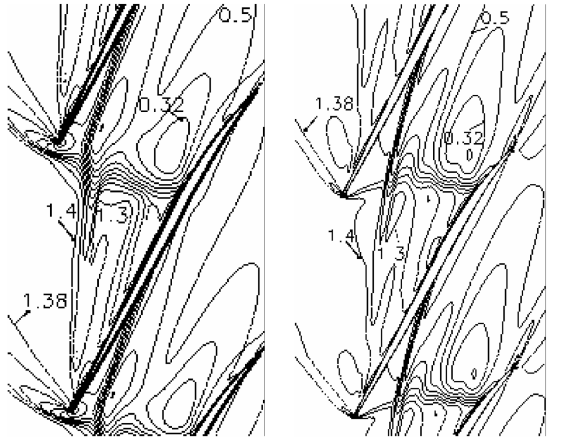

b) 75% span

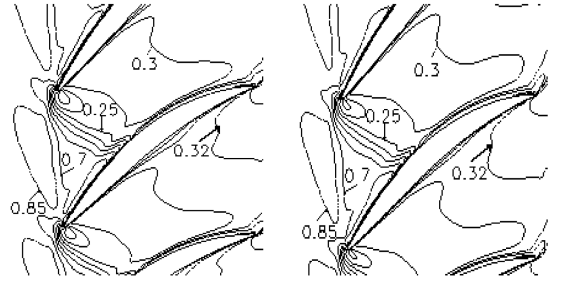

c) 10% span

Reference blade Efficiency optimized blade

Fig. 12 Mach number contours on the planes of 10, 75, and 90% span (interval of contour lines = 0.1).

the results of Jang et al. [6], who suggested that the optimization of the three-dimensional stacking line using the blade sweep, lean, and skew reduces the tip losses. Gallimore et al. [2] also reported that a positive lean reduced a hub corner and tip clearance losses except near the midspan region. Because the blade profiles are similar for total temperature ratio and total pressure ratio optimized blades, the distributions shown in Figs. 13c and 13d are also similar. Figure 14 shows the temperature distributions on suction and pressure surfaces of the reference and the optimum blades. Remarkable differences in temperature distribution are not found between the cases.

V. Conclusions

The predictive capabilities of a multiple surrogate model, PBA, as well as the individual surrogates, RSA, RBNN, and KRG, are evaluated for the optimization of a transonic axial compressor blade based on a RANS analysis. The blade shape is optimized for the enhancement of adiabatic efficiency, and temperature and pressure

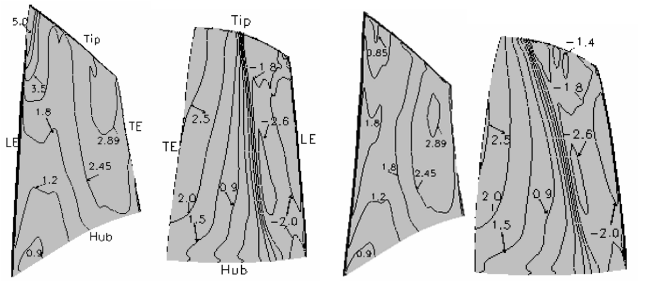

a) Reference blade **b) Efficiency optimized blade**

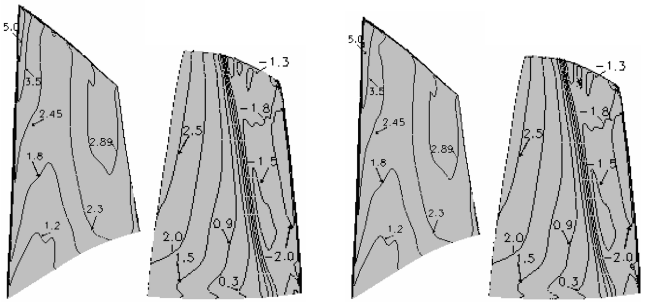

c) Pressure ratio optimized blade **d) Temperature ratio optimized blade**

Fig. 13 Pressure coefficient contours on surfaces of optimum blades.

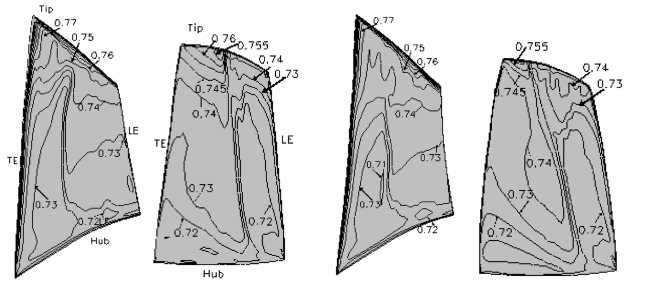

a) Reference blade **b) Efficiency optimized blade**

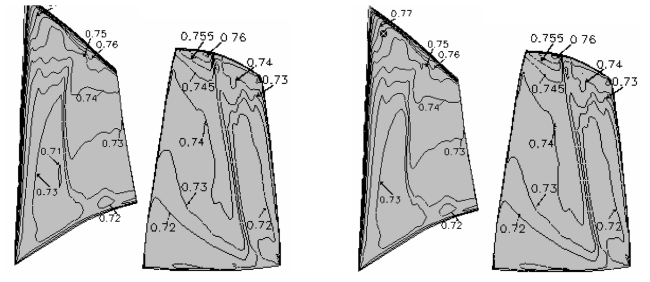

c) Pressure ratio optimized blade **d) Temperature ratio optimized blade**

Fig. 14 Temperature contours on surfaces of optimum blades.

ratios. About 1.4% of relative increase in blade efficiency is obtained. Other objective functions, that is, total temperature and total pressure ratios are also increased.

In this application, KRG gives the highest cross-validation error and performs the worst for all of the objective functions. RSA, with the lowest cross-validation error, shows the best reliability of the surrogates in some cases. However, RBNN predicts the best optimum points in all cases. Even though the weighted surrogate PBA is not the best in any case, it gives satisfactory results in most cases and protects against choosing a poor surrogate if only one is chosen. Therefore, the simultaneous application of multiple surrogate models offers enhanced robustness in the optimization process. The present approach can help address the multi-objective design on a rational basis with quantifiable cost-benefit estimates.

Appendix: Generalized Mean Square Cross-Validation Error (GMSE)

The generalized mean square cross-validation error is calculated to get the weights for weighted average methods. In general, the data are divided into k subsets (k-fold cross validation) of approximately equal size. A surrogate model is constructed k times, each time leaving out one of the subsets from training and using the omitted subset to compute the error measure of interest. The generalization error estimate is computed using the k error measures obtained (e.g., average). If k equals the sample size, this approach is called leave-one-out cross-validation (also known as PRESS in the polynomial response surface approximation terminology). The following equation represents a leave-one-out calculation when the generalization error is described by the mean square error:

$$GMSE = \frac{1}{k}\sum_{i=1}^{k}\left(f_i - \hat{f}_i^{(-i)}\right)^2$$

where $\hat{f}_i^{(-i)}$ represents the prediction at $x^{(i)}$ using the surrogate constructed with all sample points except $(x^{(i)}, f_i)$.

Acknowledgments

The authors acknowledge the support from the Korea Institute of Science and Technology Information under the Seventh Strategic Supercomputing Support Program, the Foreign Student Researcher Invitation Program of the Korean Ministry of Science and Technology (KRF-2004-410052), the NASA Constellation University Institute Program, and the National Science Foundation (grant no. DDM-423280).

References

[1] Papila, N., Shyy, W., Griffin, L., and Dorney, D. J., "Shape Optimization of Supersonic Turbines Using Global Approximation Methods," *Journal of Propulsion and Power*, Vol. 18, No. 3, 2002, pp. 509–518.

[2] Gallimore, S. J., Bolger, J. J., and Cumpsty, N. A., "The Use of Sweep and Diahedral in Multistage Axial Flow Compressor Blading, Part 1: University Research and Methods Development," ASME Paper GT-2002-30328, 2002.

[3] Ahn, C. S., and Kim, K. Y., "Aerodynamic Design Optimization of a Compressor Rotor with Navier–Stokes Analysis," *Proceedings of the Institution of Mechanical Engineers. Part A, Journal of Power and Energy*, Vol. 217, No. 2, 2003, pp. 179–184. doi:10.1243/09576500360611209

[4] Jang, C. M., and Kim, K. Y., "Optimization of a Stator Blade Using Response Surface Method in a Single-Stage Transonic Axial Compressor," *Proceedings of the Institution of Mechanical Engineers. Part A, Journal of Power and Energy*, Vol. 219, No. 8, 2005, pp. 595–603. doi:10.1243/095765005X31298

[5] Jang, C.-M., Li, P., and Kim, K. Y., "Optimization of Blade Sweep in a Transonic Axial Compressor Rotor," *Japan Society of Mechanical Engineers International Journal. Series B*, Vol. 48, No. 4, 2005, pp. 793–801. doi:10.1299/jsmeb.48.793

[6] Jang, C. M., Samad, A., and Kim, K. Y., "Optimal Design of Swept, Leaned and Skewed Blades in a Transonic Axial Compressor," ASME Paper GT2006-90384, 2006.

[7] Yi, W., Huang, H., and Han, W., "Design Optimization of Transonic Compressor Rotor Using CFD and Genetic Algorithm," ASME Paper GT2006-90155, 2006.

[8] Benini, E., and Biollo, R., "On the Aerodynamics of Swept and Leaned Transonic Compressor Rotors," ASME Paper GT2006-90547, 2006.

[9] Oyama, A., Liou, M. S., Obayashi, S., "Transonic Axial-Flow Blade Optimization: Evolutionary Algorithms/Three-Dimensional Navier–Stokes Solver," *Journal of Propulsion and Power*, Vol. 20, No. 4, 2004, pp. 612–619.

[10] Queipo, N. V., Haftka, R. T., Shyy, W., Goel, T., Vaidyanathan, R., and Tucker, P. K., "Surrogate-Based Analysis and Optimization," *Progress in Aerospace Sciences*, Vol. 41, No. 1, 2005, pp. 1–28. doi:10.1016/j.paerosci.2005.02.001

[11] Li, W., and Padula, S., "Approximation Methods for Conceptual Design of Complex Systems," *Approximation Theory XI: Gatlinburg 2004*, edited by Chui, C., M. Neaumtu, and L. Schumaker, Nashboro Press, Brentwood, TN, 2005, pp. 241–278.

[12] Shyy, W., Papila, N., Vaidyanathan, R., and Tucker, K., "Global Design Optimization for Aerodynamics and Rocket Propulsion Components," *Progress in Aerospace Sciences*, Vol. 37, No. 1, 2001, pp. 59–118. doi:10.1016/S0376-0421(01)00002-1

[13] Zerpa, L., Queipo, N. V., Pintos, S., and Salager, J., "An Optimization Methodology of Alkaline-Surfactant-Polymer Flooding Processes Using Field Scale Numerical Simulation and Multiple Surrogates," *Journal of Petroleum Science and Engineering*, Vol. 47, No. 3–4, June 2005, pp. 197–208. doi:10.1016/j.petrol.2005.03.002

[14] Goel, T., Haftka, R., Shyy, W., and Queipo, N., "Ensemble of Surrogates," *Structural and Multidisciplinary Optimization* (to be published).

[15] Goel, T., Zhao, J., Thakur, S., Haftka, R. T., and Shyy, W., "Surrogate Model-Based Strategy for Cryogenic Cavitation Model Validation and Sensitivity Evaluation," AIAA Paper 2006-5047, 2006.

[16] Reid, L., and Moore, R. D., "Design and Overall Performance of Four Highly-Loaded, High-Speed Inlet Stages for an Advanced, High-Pressure-Ratio Core Compressor," NASA TP-1337, 1978.

[17] Jameson, A., Schmidt, W., and Turkel, E., "Numerical Solutions of the Euler Equation by Finite Volume Methods Using Runge–Kutta Time Stepping Schemes," AIAA Paper 81-1259, 1981.

[18] Baldwin, B. S., and Lomax, H., "Thin Layer Approximation and Algebraic Model for Separated Turbulent Flow," AIAA Paper 78-257, 1978.

[19] Myers, R. H., and Montgomery, D. C., *Response Surface Methodology-Process and Product Optimization Using Designed Experiments*, Wiley, New York, 1995.

[20] Orr, M. J. L., *Introduction to Radial Basis Neural Networks*, Center for Cognitive Science, Edinburgh Univ., Scotland, U.K., April 1996, http://anc.ed.ac.uk/rbf/.

[21] MATLAB®, The language of technical computing, Release 14, The MathWorks, Inc., 2005.

[22] Martin, J. D., and Simpson, T. W., "Use of Kriging Models to Approximate Deterministic Computer Models," *AIAA Journal*, Vol. 43, No. 4, 2005, pp. 853–863.

F. Liu
Associate Editor